

## Physics of delamination onset in unidirectional composite laminates under mixed-mode I/II loading

Daneshjoo, Zahra; Shokrieh, Mahmood M.; Fakoor, Mahdi; Alderliesten, René; Zarouchas, Dimitrios

**DOI**

[10.1016/j.engfracmech.2019.02.013](https://doi.org/10.1016/j.engfracmech.2019.02.013)

**Publication date**

2019

**Document Version**

Final published version

**Published in**

Engineering Fracture Mechanics

**Citation (APA)**

Daneshjoo, Z., Shokrieh, M. M., Fakoor, M., Alderliesten, R., & Zarouchas, D. (2019). Physics of delamination onset in unidirectional composite laminates under mixed-mode I/II loading. *Engineering Fracture Mechanics*, 211, 82-98. <https://doi.org/10.1016/j.engfracmech.2019.02.013>

**Important note**

To cite this publication, please use the final published version (if applicable). Please check the document version above.

**Copyright**

Other than for strictly personal use, it is not permitted to download, forward or distribute the text or part of it, without the consent of the author(s) and/or copyright holder(s), unless the work is under an open content license such as Creative Commons.

**Takedown policy**

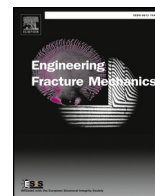
Please contact us and provide details if you believe this document breaches copyrights. We will remove access to the work immediately and investigate your claim.

***Green Open Access added to TU Delft Institutional Repository***

***'You share, we take care!' – Taverne project***

**<https://www.openaccess.nl/en/you-share-we-take-care>**

Otherwise as indicated in the copyright section: the publisher is the copyright holder of this work and the author uses the Dutch legislation to make this work public.



## Physics of delamination onset in unidirectional composite laminates under mixed-mode I/II loading

Zahra Daneshjoo<sup>a</sup>, Mahmood M. Shokrieh<sup>a,\*</sup>, Mahdi Fakoor<sup>b</sup>, René Alderliesten<sup>c</sup>, Dimitrios Zarouchas<sup>c</sup>

<sup>a</sup> Composites Research Laboratory, Center of Excellence in Experimental Solid Mechanics and Dynamics, School of Mechanical Engineering, Iran University of Science and Technology, Tehran 16846-13114, Iran

<sup>b</sup> Faculty of New Sciences and Technologies, University of Tehran, Tehran 14395-1561, Iran

<sup>c</sup> Structural Integrity & Composites Group, Faculty of Aerospace Engineering, Delft University of Technology, Kluyverweg 1, 2629HS Delft, the Netherlands

### ARTICLE INFO

#### Keywords:

Delamination  
Laminated composite  
Strain energy density  
Mixed mode I/II loading

### ABSTRACT

In order to understand the physics of the delamination onset in laminated composites, an experimental investigation of delamination growth is presented. The main objective of this paper is to demonstrate that delamination onset occurs at lower values than  $G_c$  defined by the ASTM standards, and that the strain energy release rate level at which the crack growth onset occurs under any mixed mode I/II loading is governed by the critical strain energy density (SED) approach. Quasi-static delamination experiments have been performed under mode I, mode II and mixed mode I/II loadings. The value of the strain energy release rate at the observed crack onset and the angle of the initial crack growth were correlated with the SED theory to test the validity. The acoustic emission was also used to provide more insight into the physics of the delamination growth. The investigation shows that the onset of delamination growth occurs at the strain energy release rate levels predicted by the critical SED approach, and well before reaching the critical strain energy release rate determined via delamination tests following the ASTM standards. Moreover, results indicated that the predicted angle of the initial crack for delamination onset was in a good agreement with the experimental data.

### 1. Introduction

Composite laminates are widely used in various industrial applications because of their favorable physical and mechanical properties such as high strength to weight ratio. However, the lack of reinforcement in the through-the-thickness direction makes them vulnerable to delamination, which is one of the most critical failure modes in laminated composites [1,2]. Therefore, several studies have been carried out to assess the delamination growth in composite structures [3–6]. In engineering problems, delamination growth in composites under mixed mode I/II loading is traditionally evaluated using the fracture mechanics parameters like the strain energy release rate (SERR). For design purposes, the critical strain energy release rate at the onset of delamination growth is often taken instead of the maximum value and referred to as the fracture toughness ( $G_c$ ) [7]. In the ASTM standards [8–10], the onset of damage growth is determined at one of the three points on the load-displacement plots, as shown in Fig. 1: the point of deviation from linearity (NL), the point at which the delamination growth is visually observed (VIS) or the intersection of a 5% offset line (5% Max).

\* Corresponding author.

E-mail address: [Shokrieh@iust.ac.ir](mailto:Shokrieh@iust.ac.ir) (M.M. Shokrieh).

<https://doi.org/10.1016/j.engfracmech.2019.02.013>

Received 23 September 2018; Received in revised form 2 February 2019; Accepted 7 February 2019

Available online 08 February 2019

0013-7944/ © 2019 Elsevier Ltd. All rights reserved.

Nomenclature			
$a_0$	length of the film insert which forms the starter delamination	$M$	mixed mode ratio
$c$	lever length	$P_{ini-Exp.}$	critical load at the onset of crack growth obtained via delamination experiments
$C_{ij}$	components of the compliance matrix for the plane stress conditions	$P_{ini-SED}$	critical load at the onset of crack growth calculated using the critical SED approach
$C'_{ij}$	components of the compliance matrix for the plane strain conditions	$S$	strain energy density factor
$E_i, i = x, y, z$	Young's moduli in the $i$ direction	$S_{cr}$	critical strain energy density factor
$F_I, F_{II}$	generalized elastic moduli	$\nu_{ij}$	Poisson's ratio in the $ij$ plane
$G_{ij}$	shear modulus in the $ij$ plane	$\theta$	angle from the crack tip
$G$	strain energy release rate (SERR)	$\theta_0$	crack initiation angle
$G_{Icr}, G_{IIcr}, G_{I/IIcr}$	critical SERR for the onset of mode I, mode II and mixed mode I/II delamination	$\theta_{0I}, \theta_{0II}, \theta_{0I/II}$	initial crack growth angle under mode I, mode II and mixed mode I/II loading
$G_{I/IIcr}, G_{II/I/IIcr}$	mode I and mode II components of critical SERR for the onset of mixed mode I/II delamination	AE	acoustic emission
$G_{cr Exp.}$	critical SERR for the onset of delamination growth obtained via experiments	ASTM	American society for testing and materials
$G_{cr SED}$	critical SERR for the onset of delamination growth calculated using the critical SED approach	DCB	double cantilever beam
$h$	specimen half thickness	ENF	end notched flexure
$K_I, K_{II}$	mode I and mode II stress intensity factor	MBT	modified beam theory
$L$	half-span length	MMB	mixed mode bending
		MTS	maximum tangential stress
		NL	Nonlinearity
		QS	quasi-static
		SD	standard deviation
		SED	strain energy density
		SERR	strain energy release rate
		SIF	stress intensity factor

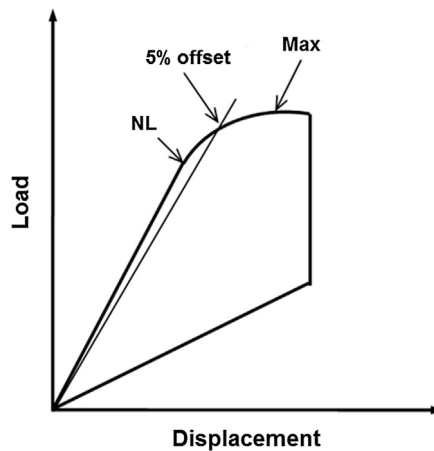


Fig. 1. Schematic of a load-displacement curve.

Although current methods satisfactorily describe the behavior of delamination growth in laminated composites, from a design point of view more understanding of the physics underlying delamination growth is required. So, the question is how to connect the fracture toughness with the underlying physics of delamination growth? This link would enable a better understanding of delamination failure, which could lead to design lighter load-bearing composite structures. In a number of research studies available in the literature, researchers [11–16] have tried to connect the macroscopic description of delamination through the SERR with the microscopic damage features, as discussed elsewhere [17,18]. To this aim, they used the SERR and fractography on the mode I and mode II interlaminar fracture surfaces to investigate the effect of different parameters such as the mode mixity, resin toughness and resin layer thickness in the delamination resistance. The general observation in these studies was that the onset fracture toughness of mode II is substantially higher than that of the mode I. A proper physical explanation for this apparent difference has never been given until recently, when Amaral et al. [19] correlated the microscopically observed onset of damage growth under mode II loading to the strain energy density in the proximity of the starter notch tip. They developed a physics-based theory based on the strain energy density to predict the load at which microscopically the crack onset occurs under mode II loading together with the initial crack growth angle. For a number of isotropic and orthotropic material cases from the literature, they demonstrated the validity of this theory in the case of the pure mode II loading. Followed by this work, Daneshjoo [20] generalized the physics-based theory for

crack growth under mixed mode I/II loading and made a similar comparison between the results of the physics-based relationships and the available experimental data in mixed mode I/II delamination growth. From these comparisons, they concluded that the onset of the pure mode II and mixed mode I/II delamination growth in laminated composites occurs at the SERR levels lower than the SERR value obtained by experiments defined in the ASTM standards ( $G_c$ ) [8–10]. Their approach in predicting the delamination growth of laminated composites was completely theoretical and was not supported by any experimental evidence.

Therefore, the main objective of this work is to examine whether in the pure mode II and mixed mode I/II delamination of laminated composites the crack growth onset actually occurs at the SERR levels lower than  $G_c$  defined by the ASTM standards [8–10]. In the present experimental work, instead of using a phenomenological linking between the fracture toughness measured by standardized tests for various mode mixities, a coherent approach was developed to demonstrate what physically happens in the damage onset under a mixed mode I/II delamination of laminated composites. The critical SED approach forms the hypothesis of the current paper, in that the strain energy density also explains the crack onset for delamination in orthotropic composite laminates under any mixed mode I/II loading. Quasi-static delamination experiments have been performed under mode I, mode II and mixed mode I/II loadings. To evaluate the theory, the value of the strain energy release rate at the observed crack onset and the angle of the initial crack growth were compared with the results of the theory. In addition, the acoustic emission (AE) technique was used to demonstrate that the energy was dissipated in a process different from the visually observed crack growth.

The tested material and the experimental technique are thoroughly described in Section 3 of the paper. In Section 4, the results are presented and discussed in the light of a theory briefly proposed in Section 2.

## 2. Strain energy density theory for crack onset in orthotropic composite laminates

Several failure theories are available for evaluating the crack growth in mixed mode I/II crack problems. The maximum tangential stress (MTS) theory [21], the maximum energy release rate ( $G$ ) theory [22] and the minimum strain energy density (SED) theory [23] are some of the well-known mixed mode failure theories. The former is a stress-based theory and the other two are energy-based ones. These failure theories were extended to orthotropic materials and modified for prediction of the mixed mode I/II delamination growth by some researchers [24–26]. Based on the MTS criterion, a mixed mode crack extends from the crack tip along the direction of the maximum tangential stress, and that crack growth occurs when the maximum tangential stress exceeds a critical value. The  $G$  criterion assumes that the crack extension occurs at the crack tip in a radial direction along which the energy release is a maximum, and the critical value of this energy release rate governs the onset of crack propagation. According to the SED criterion, the crack initiation will start in a radial direction along which the strain energy density is a minimum, and when the strain energy density at some distance from the crack tip in this direction reaches a critical value, the crack starts to propagate.

Although these theories seem plausible for predicting the onset of the crack growth under mixed mode I/II loading, the criterion gaining the most acceptance if it is able to make a better prediction. So, certain researchers have a preference for one theory over another simply because it fits better with the data. However, when one is aiming at the physics, the ‘best fit’ is not the requirement, but preference is given to theories that somehow find their base in physics.

Since the complete stress functions and the contribution of stresses in all directions are considered through the strain energy density function, the SED criterion provides a more complete description of damage in the crack tip zone on physical grounds [19,27]. Thus, in the current paper, the SED criterion is adopted instead of other theories for investigation of the physics behind the delamination onset in orthotropic composite laminates under mixed mode I/II loading.

In a series of investigations on fracture mechanics, Sih [23] has proposed a theory of fracture based on the local strain energy density around the crack tip. The fundamental parameter in SED theory, the strain energy density factor ( $S$ ), in a linear elastic orthotropic laminate is defined as follows [28]:

$$S = D_1 K_I^2 + D_2 K_{II}^2 + 2D_3 K_I K_{II} \quad (1)$$

The coefficients  $D_1$ ,  $D_2$  and  $D_3$  are described in Appendix A.

The SED criterion states that:

- (1) The onset of the crack growth takes place in the direction  $\theta_0$  along which the strain energy density factor is a minimum.

$$\frac{\partial S}{\partial \theta} = 0 \text{ and } \frac{\partial^2 S}{\partial \theta^2} > 0 \text{ at } \theta = \theta_0 \quad (2)$$

- (2) The crack growth occurs once the minimum strain energy density factor has attained a critical value.

$$S_{\min} = S_{cr} \text{ at } \theta = \theta_0 \quad (3)$$

From the perspective of physics, the onset of the crack growth is expected to occur when the strain energy available in a limited volume near the crack tip reaches a critical value. Hence, rather than a phenomenological consideration of stress as a ‘driving quantity’, the physics-based aspect here is considered by the strain energy density concept. The strain energy density function by considering the complete stress functions and functions that describe the stress distribution can characterize the energy dissipation during the fracture phenomenon, and so completely describe the physics of the fracture. The critical strain energy density factor ( $S_{cr}$ ) for the onset of crack growth can be used as an intrinsic material parameter whose value is independent of loading conditions and the crack configuration [29]. Amaral et al. [19] recently used this hypothesis to develop a physics-based theory for the onset of the crack

growth. According to their approach, namely the critical strain energy density approach described in detail in [19], the critical SED necessary for the crack onset under pure mode I loading is the same as the critical SED necessary for the crack onset under pure mode II loading.

$$S_{Icr} = S_{IIcr} \tag{4}$$

They applied the critical SED approach to investigate the delamination growth in orthotropic composite laminates [19]. However, the reader should note that this includes an approximation. The expressions of the SED theory were developed for orthotropic homogeneous materials while the composites are obviously not homogeneous. Hence, a first approximation is to consider the resin rich layer as ‘sort of homogeneous’, but that the adjacent fiber orientations dominate the orthotropic state. Actually, when the orthotropic state is explicitly captured in the formulations for SED, the approach is deemed valid for the limit of  $a \geq 0$ , because that the earliest moment of the crack length onset is in a ‘sort of homogeneous’ material. Since this moment or level of this onset and the initial direction are defined at that moment, it should be approximately correct, indifferent the simplicity of the approach. Since the calculation of stress intensity factors (SIFs) for composite materials is not straightforward, the strain energy density factor ( $S$ ) was written in terms of the strain energy release rate (SERR) using the following relation for composite materials under the plane strain conditions [28].

$$\begin{aligned} G_I &= F_I K_I^2 \quad (\text{Mode I}) \\ G_{II} &= F_{II} K_{II}^2 \quad (\text{Mode II}) \end{aligned} \tag{5}$$

in which:

$$\begin{aligned} F_I &= \left[ \frac{C'_{11} C'_{22}}{2} \left( \sqrt{\frac{C'_{22}}{C'_{11}}} + \frac{2C'_{12} + C'_{66}}{2C'_{11}} \right) \right]^{1/2} \\ F_{II} &= \left[ \frac{C'^2_{11}}{2} \left( \sqrt{\frac{C'_{22}}{C'_{11}}} + \frac{2C'_{12} + C'_{66}}{2C'_{11}} \right) \right]^{1/2} \end{aligned} \tag{6}$$

where the coefficients  $C'_{11}$ ,  $C'_{22}$ ,  $C'_{12}$  and  $C'_{66}$  are given in Appendix A. Substituting SIFs from Eq. (5) into Eq. (1) gives:

$$S = D_1 \frac{G_I}{F_I} + D_2 \frac{G_{II}}{F_{II}} + 2D_3 \left( \frac{G_I G_{II}}{F_I F_{II}} \right)^{1/2} \tag{7}$$

Applying the conditions stated in Eqs. (2)–(7) in the case of pure mode I delamination, it was found [19] that the angle which makes the function  $D_1$  a minimum is the initial crack growth angle under pure mode I loading ( $\theta_{0I}$ ). In this case, the minimum value of  $S$  was found to be:

$$S_{Icr} = D_1(\theta_{0I}) \frac{G_{Icr}}{F_I} \tag{8}$$

where  $G_{Icr}$  is the critical SERR for the onset of mode I delamination.

In the case of the pure mode II, the critical value of  $S$  was given:

$$S_{IIcr} = D_2(\theta_{0II}) \cdot \left( \frac{G_{IIcr}}{F_{II}} \right) \tag{9}$$

where the function  $D_2$  reaches its minimum at  $\theta_{0II}$  and  $G_{IIcr}$  is the critical SERR for the onset of mode II delamination. Substituting of Eqs. (8) and (9) into Eq. (4), the mode II critical SERR was obtained by the mode I critical SERR and material properties as follows [19]:

$$G_{IIcr} = G_{Icr} \cdot \left( \frac{F_{II} \cdot D_1(\theta_{0I})}{F_I \cdot D_2(\theta_{0II})} \right) \tag{10}$$

Daneshjoo [20] developed the critical strain energy density approach for mixed mode I/II crack growth and extracted the generalized physics-based theory under any mixed mode I/II loading. According to the critical strain energy density approach:

$$S_{Icr} = S_{I/IIcr} \tag{11}$$

For mixed mode I/II delamination, applying conditions of Eqs. (2)–(7) and using mixed mode ratio defined as  $G_{II}/G_I = G_{II}/G_I + G_{II} = M$ , it was found [20] that the angle in which the function  $D$  in Eq. (12) has a minimum value is the initial crack growth angle under mixed mode I/II loading ( $\theta_{0I/II}$ ).

$$D = D_1 + \left( \left( \frac{M}{1-M} \right) \left( \frac{F_I}{F_{II}} \right) D_2 \right) + \left( 2 \left( \frac{M}{1-M} \right)^{1/2} \left( \frac{F_I}{F_{II}} \right)^{1/2} D_3 \right) \tag{12}$$

So, the initial crack growth angle ( $\theta_{0I/II}$ ) was obtained as a function of material properties and mixed-mode ratio.

$$\theta_{0I/II} = p(\nu_{ij}, E_i, G_{ij}, M) \quad i, j = x, y, z \tag{13}$$

Using the relation of mixed-mode ratio and substituting  $\theta_{0I/II}$  in Eq. (13) into Eq. (7), the critical value of  $S$  under the mixed mode I/II loading was given by:

$$S_{I/II_{cr}} = G_{I/II_{cr}} \left[ \frac{D_1(\theta_{0I/II})}{F_I} + \left(\frac{M}{1-M}\right) \frac{D_2(\theta_{0I/II})}{F_{II}} + 2\left(\frac{M}{1-M}\right)^{1/2} \left(\frac{1}{F_I F_{II}}\right)^{1/2} D_3 \right] \tag{14}$$

where  $G_{I/II_{cr}}$  is the mode I component of critical SERR for the onset of the mixed mode I/II delamination.

A substitution of Eqs. (8) and (14) into Eq. (11) yielded to the extraction of mode I and II components of the critical SERR under mixed mode I/II loading ( $G_{I/II_{cr}}$  and  $G_{II/II_{cr}}$ ) from the mode I critical SERR, material properties and mixed-mode ratio.

$$\frac{G_{I/II_{cr}}}{G_{I_{cr}}} = \left( \frac{D_1(\theta_{0I})}{D_1(\theta_{0I/II}) + \left(\frac{M}{1-M}\right) \left(\frac{F_I}{F_{II}}\right) D_2(\theta_{0I/II}) + 2\left(\frac{M}{1-M}\right)^{1/2} \left(\frac{F_I}{F_{II}}\right)^{1/2} D_3(\theta_{0I/II})} \right) = q(\nu_{ij}, E_i, G_{ij}, M) \tag{15}$$

So,

$$\begin{aligned} G_{I/II_{cr}} &= G_{I_{cr}} \cdot q(\nu_{ij}, E_i, G_{ij}, M) \\ G_{II/II_{cr}} &= G_{I/II_{cr}} \cdot \left(\frac{M}{1-M}\right) = G_{I_{cr}} \cdot q(\nu_{ij}, E_i, G_{ij}, M) \cdot \left(\frac{M}{1-M}\right) \rightarrow G_{I/II_{cr}} = G_{I/II_{cr}} + G_{II/II_{cr}} \end{aligned} \tag{16}$$

In the above equations  $0 \leq M < 1$  where  $M = 0$  and  $M = 1$  denote pure mode I and pure mode II loading conditions, respectively. More details of the critical SED approach are available in [19,20].

The results of these physics-based relationships in the case of the pure mode II loading were compared with the available experimental data by Amaral et al. [19]. Also, using the available data in the literature for orthotropic composite laminate, Daneshjoo [20] made a similar comparison in the mixed mode I/II delamination growth. According to these two studies [19,20], it was found out that:

- In the pure mode II and mixed mode I/II delamination of laminated composites, the critical SED approach predicts that the initial crack growth onset occurs at the SERR levels ( $G_{cr|SED}$ ) lower than the  $G_{cr|Exp.}$  value obtained by experiments defined in the ASTM standards [8–10]. This difference is attributed to the presence of the mode II loading that develops a fracture process zone by the formation of cusps and micro-cracks ahead of the crack tip.
- The critical SED approach can be used to predict the load at which microscopically the crack onset occurs together with the initial crack growth angle.

In order to evaluate the validity of the critical SED approach in predicting the delamination growth of orthotropic composite laminates, an experimental investigation is presented in the next section. Some experiments have been performed under mode I, mode II and mixed mode loading, and the value of the strain energy release rate at the observed crack onset and the angle of the initial crack are compared with the results of the theory.

### 3. Experimental procedure

#### 3.1. Materials and test specimens

Two types of composites, i.e., carbon/epoxy and glass/epoxy laminated composites were manufactured. The carbon/epoxy composite laminates were produced by the hand-lay-up of 32 unidirectional carbon/epoxy prepreg layers of the same material batch, M30SC-150/DT 120-34F. A 15 μm FEP film was inserted in the mid-plane of carbon/epoxy laminates as the delamination starter. The carbon/epoxy laminates were cured in an autoclave at a pressure of 6 bars and a curing temperature of 120 °C for 90 min. This cure cycle was recommended by Delta Tech as the manufacturer. For glass/epoxy laminates, 18 layers of unidirectional E-glass fiber were used together with EPON 826 epoxy resin to manufacture composite laminates by the hand-lay-up method. A thin film-insert with a thickness of 20 μm was used to form an initiation site for the delamination. The glass/epoxy laminates were cured at room temperature for 7 days and post-cured at 150 °C for 120 min. The both cured laminates were C-scanned to detect potential imperfections. Afterward, specimens with a width of 25 mm were cut from the defect-free portions of the laminates by a water jet cutting machine. The elastic properties of both unidirectional laminates are presented in Tables 1 and 2. In this study, there are three types of specimens, i.e., double cantilever beam (DCB), mixed mode bending (MMB) and end notched flexure (ENF) specimens with the nominal dimensions shown in Fig. 2. All of the carbon/epoxy and glass/epoxy specimens have a total thickness of 5 mm and 4.1 mm, respectively. The edges of the specimens were sanded with sandpaper. Then, one edge of each specimen was coated with a thin white water-based correction fluid to enhance the delamination tip detection and the other edge was polished with a diamond paste having sized grits equal to 6, 3 and 1 μm successively to remove machining marks. Aluminum end blocks were adhesively bonded to the specimens to facilitate its fastening with hinges.

**Table 1**  
Elastic properties of M30SC-150/DT 120-34F carbon/epoxy system [30].

Laminated composite material	$E_x$ (GPa)	$E_y$ (GPa)	$E_z$ (GPa)	$G_{xy}$ (GPa)	$G_{xz}$ (GPa)	$G_{yz}$ (GPa)	$\nu_{xy}$	$\nu_{xz}$	$\nu_{yz}$
M30SC-150/DT 120-34F	155	7.8	7.8	5.50	5.50	3.92	0.290	0.290	0.487

**Table 2**  
Elastic properties of unidirectional E-glass/EPON 826 epoxy [31].

Laminated composite material	$E_x$ (GPa)	$E_y$ (GPa)	$E_z$ (GPa)	$G_{xy}$ (GPa)	$G_{xz}$ (GPa)	$G_{yz}$ (GPa)	$\nu_{xy}$	$\nu_{xz}$	$\nu_{yz}$
E-glass/EPON826	35.25	10.82	10.82	4.28	4.28	3.58	0.27	0.27	0.51

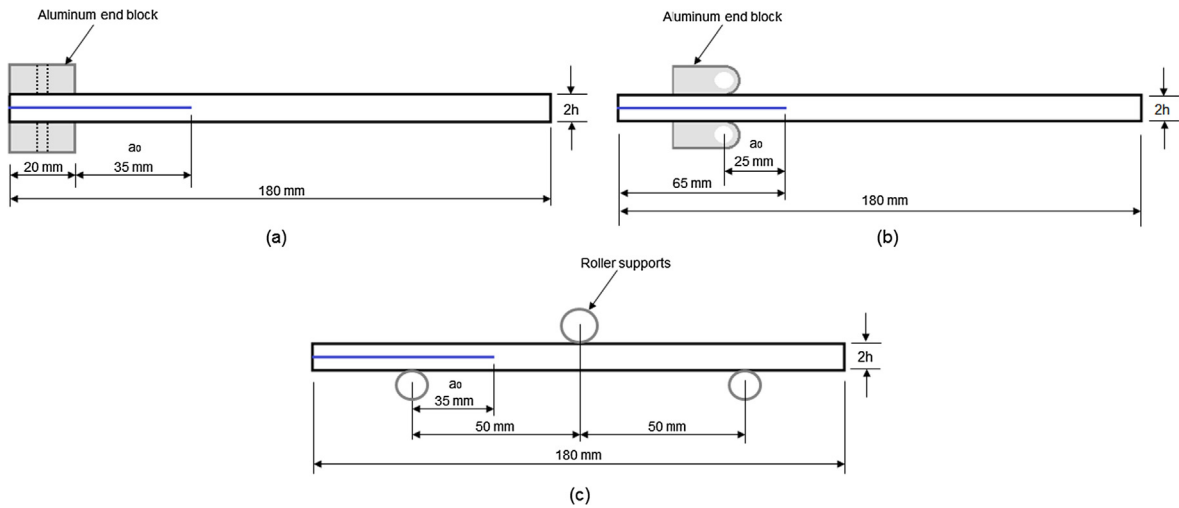


Fig. 2. Geometry and dimensions of (a) DCB, (b) MMB and (c) ENF specimens.

3.2. Test procedure

In order to investigate the delamination failure of laminated composites under pure mode I, mixed mode I/II and pure mode II loadings, double cantilever beam (DCB), mixed mode bending (MMB) and end notched flexure (ENF) test procedures were utilized, respectively. Five mode mixities defined as the ratio of mode II SERR over the total SERR, i.e.,  $G_{II}/G = 0, 0.25, 0.5, 0.75$  and  $1$  were chosen. At least three samples of both carbon/epoxy and glass/epoxy specimens were tested for each configuration.

The DCB tests were performed on a 15 kN hydraulic MTS machine according to the ASTM D5528 [8]. These tests were carried out under displacement control condition with an applied displacement rate of 1 mm/min.

The MMB specimens were tested using an MTS machine equipped with a 10 kN load-cell. The test set-up was designed according to ASTM D6671 [9]. These tests were conducted under the displacement control at a rate of 0.5 mm/min. In order to change the mixed mode ratio, the position of the yoke calculated according to the ASTM standard was adjusted for each mixed-mode ratio. The lever length used for each mode mixity is listed in Table 3 for both carbon/epoxy and glass/epoxy specimens. Moreover, the half-span length was considered to be constant ( $L = 50$  mm).

For the ENF tests, a 20 kN tensile-compression Zwick machine, under displacement control condition, was used to test the specimens based on ASTM D7905 [10]. A low crosshead speed of 0.1 mm/min was applied to slow-down the delamination propagation and to increase the number of data points.

The experimental setups for DCB, MMB and ENF tests are shown in Fig. 3. In all tests, a digital camera positioned alongside the specimen edge and a computer system was employed to monitor the delamination growth initiation by an automatic recording of the image of the specimen edge at every certain number of seconds. The load-displacement curve ( $P-\delta$ ) was recorded by the testing machine. The value of the load at delamination onset was determined from the extracted load-displacement plots. This value corresponds to the point of deviation from linearity, or onset of nonlinearity (NL), recommended in ASTM standard. Also, the measurement of initial crack growth angles was performed in a post-test analysis of the pictures, using an open source image processing program, ImageJ [32]. It should be noted that the testing procedure does not include pre-cracking by the initial loading process, and

**Table 3**  
Positions of the yoke on the MMB test fixture.

Mode mixity, $G_{II}/G$	Lever length, $c$ (mm)	
	Carbon/epoxy	Glass/epoxy
0.25	72.0	77.0
0.50	40.0	42.0
0.75	28.5	29.0

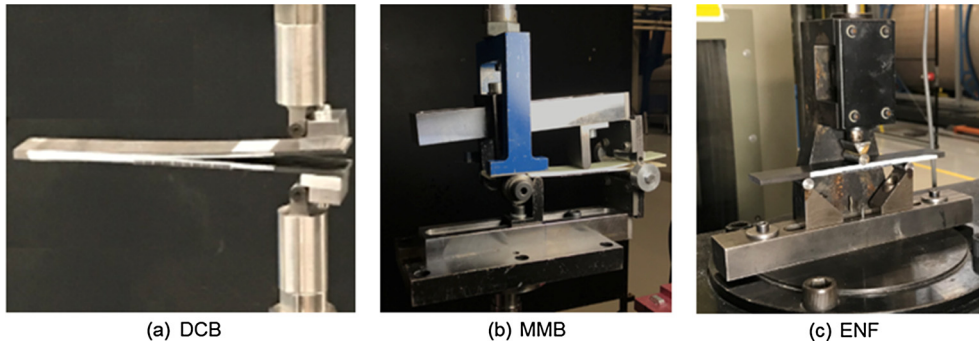


Fig. 3. Experimental setups for (a) DCB, (b) MMB and (c) ENF tests.

the calculations assume that the delamination starts to grow from the insert. In this case, the crack onset is not influenced by the fiber bridging as that will come later.

The delamination tests were performed by determining the delamination load onset as a critical load. The definition of this critical load needs to be commented; since according to critical SED approach described in Section 2 it was claimed that the value of SERR obtained via experiments following the ASTM standards [8–10] at this critical load does not refer to the onset of crack growth. It refers to the coalescence of micro-cracks ahead of the crack tip due to the presence of the mode II loading. So, the onset of delamination occurs before reaching this critical load determined via experimental tests defined in the ASTM standards [8–10]. The critical load obtained via delamination experiments, which is calculated only after coalescence has happened, is from now on referred to as  $P_{ini-Exp.}$ . Meanwhile, the critical load for the onset of mixed mode I/II and mode II crack growth, determined by the critical SED approach, is referred to as  $P_{ini-SED}$ .

To investigate the validity of the critical SED approach, at least two samples of both carbon/epoxy and glass/epoxy specimens were tested for each configuration and examined using a digital microscope. The DCB, MMB and ENF test procedures were similar as described above. The delamination tests were stopped after the load reached a value between  $P_{ini-SED}$  and  $P_{ini-Exp.}$ . After the test, the specimen was held open under this load. A thin steel plate was inserted to keep the specimen open after the test. This technique was adopted to ensure that micro-cracks are open and visible when inspected under the microscope. The polished edges of the specimens were examined using the digital microscope VHX-2000E (Keyence) to check whether the delamination onset happens.

Towards this, acoustic emission (AE) can give a better insight into the crack growth process during the delamination tests. So, the quasi-static tests were also monitored with an acoustic emission system. An AMSY-6 Vallen, 8-channel AE system with 4 parametric inputs was used. A wide-band piezoelectric sensor, AE1045S, with an external 34 dB pre-amplifier and a band-pass filter of 20–1200 kHz was clamped to the specimens as shown in Fig. 4. In all tests, a sampling rate of 2 MHz and a threshold of 50 dB<sub>AE</sub> were applied. A coupling gel was used to increase the conductivity between the sensor and the specimen. Pencil break tests were conducted before every test to ensure the conductivity. Two parametric input channels were used to record the load and displacement and correlate them to the AE activity.

It is worth remarking that the AE technique is not the main subject of the present study. The intention of using AE in this study is just for demonstrating that energy is dissipated in a process different than the visually observed crack growth [33]. Since damage formation and propagation are known to involve the energy dissipation, it seemed logical to investigate the AE energy as the characterizing parameter.

Table 4 shows an overview of the different experimental tests performed in the present work. All of the experimental data is available in the online dataset [34].

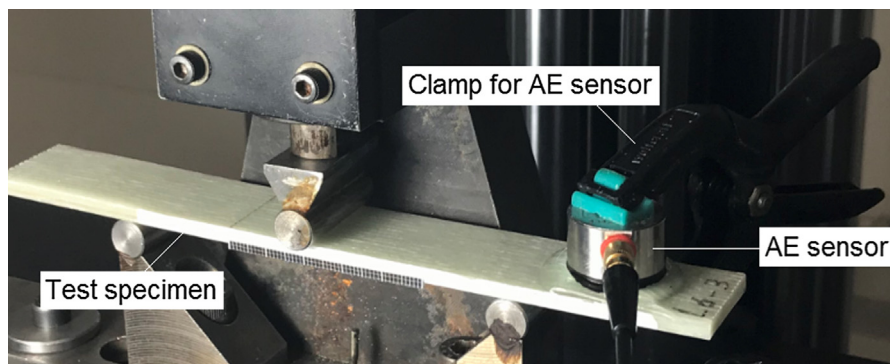


Fig. 4. Setup of the AE system of the ENF test.

**Table 4**  
Test matrix.

Number of tests	Load case	Mode mixity, $G_{II}/G$
3	Quasi-static (QS) loading at 1 mm/min on DCB specimens together with AE system until steady-state crack growth	0.00
3	QS loading at 0.5 mm/min on MMB specimens together with AE system until steady-state crack growth	0.25
3	QS loading at 0.5 mm/min on MMB specimens together with AE system until steady-state crack growth	0.50
3	QS loading at 0.5 mm/min on MMB specimens together with AE system until steady-state crack growth	0.75
3	QS loading at 0.1 mm/min on ENF specimens together with AE system until steady-state crack growth	1.00
2	QS loading at 1 mm/min on DCB specimens until load between $P_{ini-SED}$ and $P_{ini-Exp}$ , then holding the displacement and stop the test	0.00
2	QS loading at 0.5 mm/min on MMB specimens until load between $P_{ini-SED}$ and $P_{ini-Exp}$ , then holding the displacement and stop the test	0.25
2	QS loading at 0.5 mm/min on MMB specimens until load between $P_{ini-SED}$ and $P_{ini-Exp}$ , then holding the displacement and stop the test	0.50
2	QS loading at 0.5 mm/min on MMB specimens until load between $P_{ini-SED}$ and $P_{ini-Exp}$ , then holding the displacement and stop the test	0.75
2	QS loading at 0.1 mm/min on ENF specimens until load between $P_{ini-SED}$ and $P_{ini-Exp}$ , then holding the displacement and stop the test	1.00

**4. Results and discussion**

As explained in the previous section, the quasi-static delamination tests were performed on DCB, MMB and ENF specimens. Typical load-displacement curves of both carbon/epoxy and glass/epoxy specimens at five mode mixities,  $G_{II}/G = 0, 0.25, 0.50, 0.75$  and 1 are presented in Fig. 5(a) and (b). As expected, the load-displacement behavior of specimens is significantly affected by the mode mixity values. The values of load at the nonlinear point on the load-displacement curves, i.e. the  $P_{ini-Exp}$  values are summarized in Table 5. These values are used to calculate the SERR at the initiation of delamination growth ( $G_{cr|Exp}$ ) based on the modified beam theory (MBT) method in ASTM standards [8–10], which are both listed in Table 5.

Regarding the initial crack growth angles predicted for the onset of delamination, correlations with the angles measured using the images taken during experimental tests can also be made. Several examples of the initial crack growth angle in delamination of the carbon/epoxy, and glass/epoxy laminated composites under pure mode I, mixed mode I/II and pure mode II are illustrated in Fig. 6(a)–(e). These experimental values of initial crack growth angles ( $\theta_{0|Exp}$ ) are compared with the theoretical values in which the functions  $D_1$ ,  $D_2$  and  $D$  are minimum as predicted initial crack growth angle under pure mode I, pure mode II and mixed mode I/II delamination ( $\theta_{0|SED}$ ) in Table 6. The results presented in Table 6 indicate that the prediction of the angle of the initial crack for delamination onset is in good agreement with experimental data in both carbon/epoxy and glass/epoxy specimens.

It is worth noting that the limited thickness of the resin rich layer (and thus the onset crack length) limits the resolution of the measurements. It has been tried to make that more explicit by adding the “ ± x” to all the measured angles in Table 6 which has been determined based on the standard deviation (SD) from multiple measurements of repeated tests.

Using the critical SED approach, the values of critical SERR for the onset of delamination growth ( $G_{cr|SED}$ ) in different mode mixities are calculated by solving Eq. (10) for pure mode II delamination and Eqs. (15) and (16) for mixed-mode I/II delamination numerically and having the material properties and  $G_{Icr}$  given in Table 5.

According to the MBT method for calculating SERR values [8–10], SERR is proportional to the squared of the load, hence:

$$\frac{G_{cr|SED}}{G_{cr|Exp}} = \left( \frac{P_{ini-SED}}{P_{ini-Exp}} \right)^2 \tag{17}$$

Accordingly, the critical load values for the onset of delamination growth based on the critical SED approach ( $P_{ini-SED}$ ) can be determined through Eq. (17). The results obtained by numerically solving Eqs. (10), (15) and (16) and finding  $P_{ini-SED}$  from Eq. (17) are reported in Table 7.

A comparison of results summarized in Tables 5 and 7 shows that the critical SED approach predicts that an initial crack occurs for pure mode II and mixed mode I/II delamination at the SERR levels ( $G_{cr|SED}$ ) lower than the  $G_{cr|Exp}$  value obtained via experimental tests following the ASTM standards [8–10], as well as the load at which microscopically the crack onset occurs. This difference can be attributed to the presence of mode II loading that develops a fracture process zone by the formation of cusps and micro-cracks ahead of the crack tip.

The reader should note that the critical SED approach presented here is for unidirectional laminated composites. In the case of different lay-ups, since the effective material properties change, the critical SED approach for the onset of delamination growth will also change (e.g., see Eqs. (10), (15) and (16)). Although the delamination growth onset is a matrix dominated failure, the SED around the crack tip is the contribution of how the stresses, and so the strain energy is distributed ahead of the crack tip. This distribution changes once the effective properties of the laminated composite change.

Now, the question arises as for how to verify that the onset of the pure mode II and mixed mode I/II delamination growth actually occurs at  $G_{cr|SED}$ , not at  $G_{cr|Exp}$ ?

In order to investigate the validity of the critical SED approach, DCB, MMB, and ENF tests were conducted on both carbon/epoxy and glass/epoxy specimens until reaching the load value between  $P_{ini-SED}$  and  $P_{ini-Exp}$ . Some images taken from the edge of the

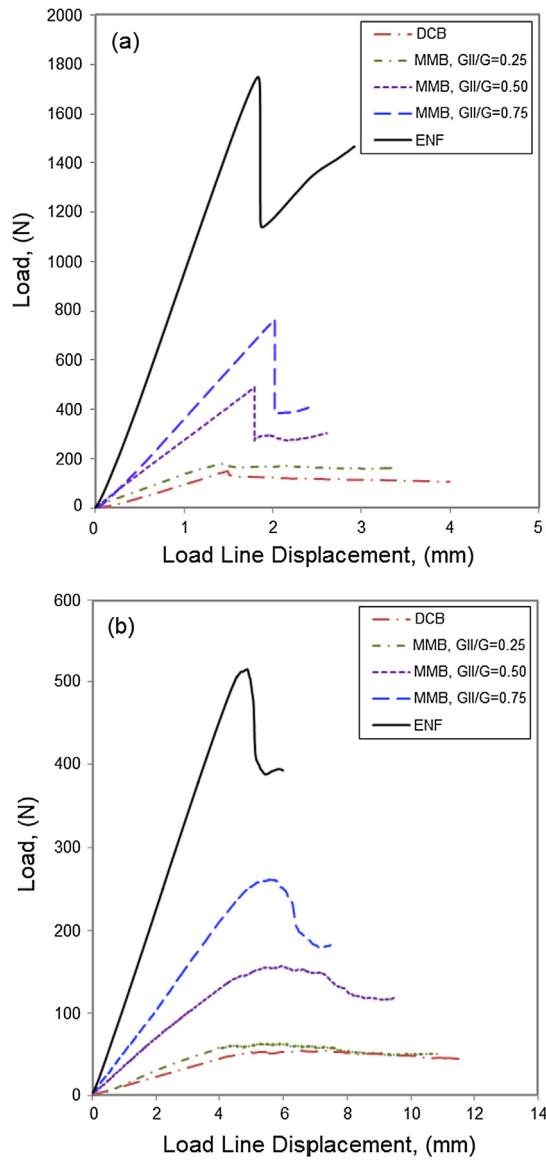


Fig. 5. Load-displacement curves of (a) carbon/epoxy and (b) glass/epoxy specimens at different mode mixities.

Table 5

The values of load at delamination onset obtained via delamination experiments and calculated critical SERR.

Loading state	Mode mixity, $G_{II}/G$	Carbon/epoxy specimen <sup>*</sup>		Glass/epoxy specimen <sup>*</sup>	
		$P_{ini-Exp.}$ (N)	$G_{cr/Exp.}$ (J/m <sup>2</sup> )	$P_{ini-Exp.}$ (N)	$G_{cr/Exp.}$ (J/m <sup>2</sup> )
Pure mode I	0.00	138.615 ( ± 1.06)	241.409 ( ± 5.65)	38.615 ( ± 4.32)	130.656 ( ± 5.12)
Mixed mode	0.25	153.348 ( ± 0.01)	357.779 ( ± 4.12)	41.294 ( ± 6.54)	273.707 ( ± 7.48)
Mixed mode	0.50	453.858 ( ± 0.01)	493.506 ( ± 9.87)	87.134 ( ± 0.64)	505.533 ( ± 1.67)
Mixed mode	0.75	693.246 ( ± 0.04)	626.416 ( ± 6.18)	160.988 ( ± 8.84)	823.813 ( ± 3.46)
Pure mode II	1.00	1719.121 ( ± 0.07)	971.115 ( ± 12.86)	489.464 ( ± 8.42)	1695.535 ( ± 9.84)

\* Mean values and standard deviations (SD, in parentheses) from multiple measurements of repeated tests.

carbon/epoxy and glass/epoxy specimens examined in the digital microscope are shown in Fig. 7(a)–(e). In the case of the pure mode I, no initial crack onset was found on the edge of the specimens until the DCB test was stopped before  $P_{ini-Exp.}$ . Fig. 7(a) shows the edge of the glass/epoxy DCB specimen exactly after  $P_{ini-Exp.}$ . As one can see, the initial crack onset is accompanied by the delamination growth. This is consistent with the assumption that the value of critical load at mode I delamination onset predicted by the

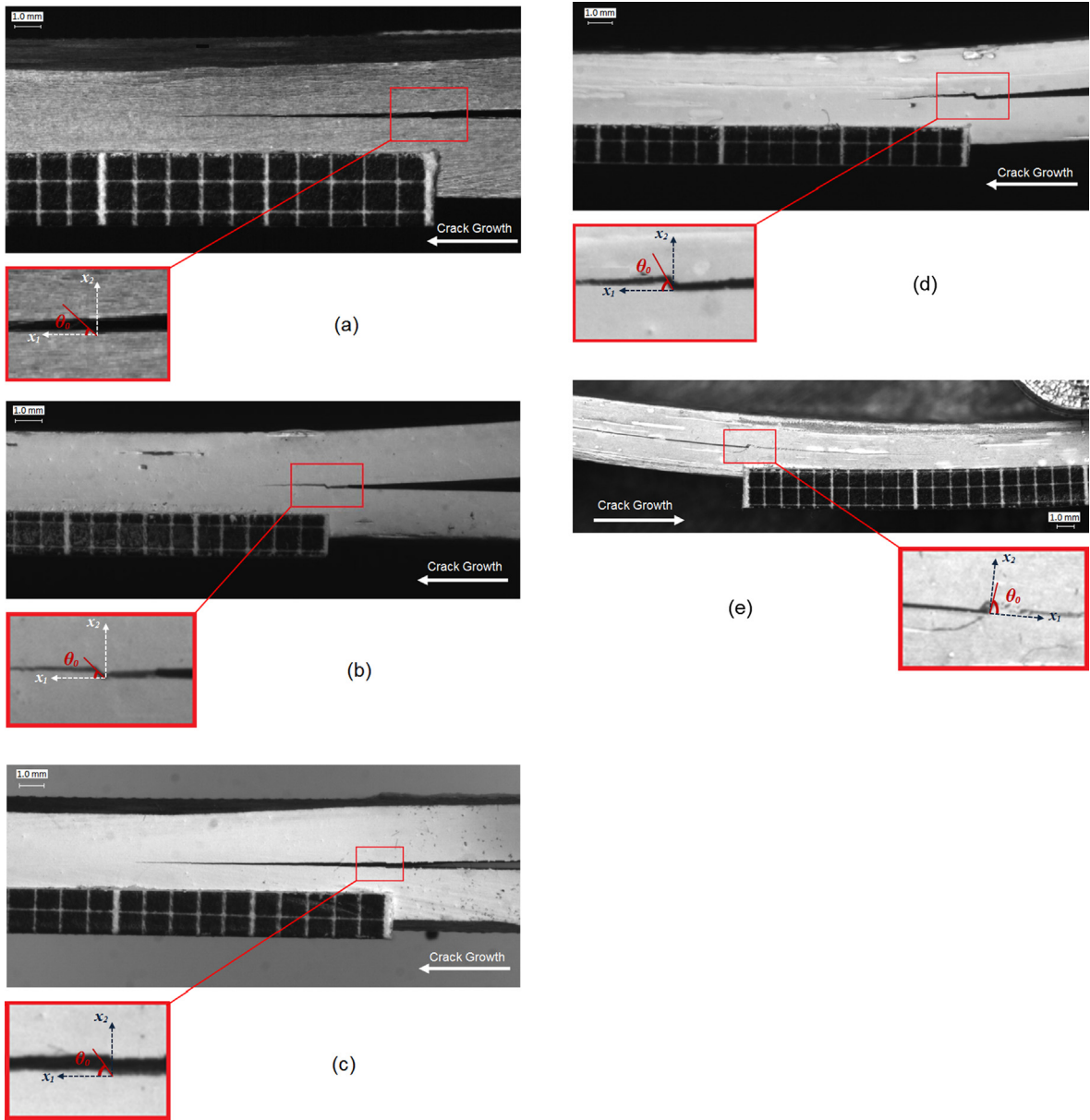


Fig. 6. Initial crack growth angle in delamination of (a) carbon/epoxy laminated composite under pure mode I, (b) glass/epoxy laminated composite under mixed mode I/II (25%  $G_{II}/G$ ), (c) carbon/epoxy laminated composite under mixed mode I/II (50%  $G_{II}/G$ ), (d) glass/epoxy laminated composite under mixed mode I/II (75%  $G_{II}/G$ ) and (e) glass/epoxy laminated composite under pure mode II.

Table 6

A comparison between estimated values of the initial crack growth angle by the critical SED approach and experimental values.

Loading state	Mode mixity, $G_{II}/G$	Carbon/epoxy specimen		Glass/epoxy specimen	
		$-\theta_0 _{SED} (^{\circ})$	$-\theta_0 _{Exp.} (^{\circ})^*$	$-\theta_0 _{SED} (^{\circ})$	$-\theta_0 _{Exp.} (^{\circ})^*$
Pure mode I	0.00	42.21	41.76 ( ± 4.98)	31.76	34.16 ( ± 8.18)
Mixed mode	0.25	45.72	47.60 ( ± 7.32)	43.23	45.97 ( ± 4.23)
Mixed mode	0.50	53.62	56.02 ( ± 8.46)	52.37	51.71 ( ± 7.58)
Mixed mode	0.75	61.73	65.46 ( ± 6.68)	61.52	60.26 ( ± 9.42)
Pure mode II	1.00	79.61	84.10 ( ± 5.65)	81.27	83.38 ( ± 6.23)

\* Mean values and standard deviations (SD, in parentheses) from multiple measurements of repeated tests.

**Table 7**

The values of critical SERR and load at delamination onset predicted by critical SED approach.

Loading state	Mode mixity, $G_{II}/G$	Carbon/epoxy specimen		Glass/epoxy specimen	
		$P_{ini-SED}$ (N)	$G_{cr SED}$ (J/m <sup>2</sup> )	$P_{ini-SED}$ (N)	$G_{cr SED}$ (J/m <sup>2</sup> )
Pure mode I	0.00	138.615	241.409	38.615	130.656
Mixed mode	0.25	114.959	201.072	27.078	117.694
Mixed mode	0.50	281.611	190.000	39.929	106.162
Mixed mode	0.75	384.735	192.936	56.461	101.329
Pure mode II	1.00	891.625	261.230	130.421	120.383

critical SED approach is the same as the critical load obtained via mode I delamination experiments. However, under the mixed mode I/II loading and pure mode II loading, an initial crack onset is clearly visible at the edges of the MMB and ENF specimens loaded until a value between  $P_{ini-SED}$  and  $P_{ini-Exp}$ . (Fig. 7(b)–(e)). In addition, after crossing  $P_{ini-SED}$  and the onset of the initial small crack, a number of micro-cracks are formed in front of the main crack tip by approaching  $P_{ini-Exp}$ . This micro-cracks formation is demonstrated in Fig. 7(c) and (d) in which the test was stopped at a load value close to  $P_{ini-Exp}$ . These observations confirm that the onset of mixed mode I/II and pure mode II delamination growth occurs before the  $G_{cr|Exp}$  value. So, the critical SED approach correctly predicts an initial crack occurring in mixed mode I/II and pure mode II delamination around the  $G_{cr|SED}$  value.

According to the experiments presented above, it is concluded that the critical SERR obtained via DCB tests refers to the onset of mode I delamination growth, while the critical SERR obtained via MMB and ENF tests refers to the coalescence of micro-cracks ahead of the crack tip. In both mixed-mode I/II and mode II delamination growth, the presence of mode II leads to the development of a process zone including the formation of micro-cracks and cusps. Only once these micro-cracks coalesce, the macroscopic crack growth can be observed from the edge of the specimen and a deviation from linearity (nonlinearity point) is observed in the load-displacement history. After reaching the maximum load and crack propagation, a load drop occurs. This is illustrated in Fig. 8(a)–(d). No load drops were observed before the maximum load in delamination tests. When the initial crack onset predicted by the critical SED approach occurs, a small load drop happened in the load-displacement curve. An example of this load drop at the moment the initial crack occurs was shown in the PVC foam rail shear tests [19]. Since this load drop was very small and captured only with a high sampling rate, it is reasonable to say that this load drop is not obvious in delamination tests. Fig. 8(a) demonstrates that the initial crack onset occurs when the load passes through  $P_{ini-SED}$ , and no load drop was observed in the load-displacement curve. This initial crack onset was not visible through observation of the edges of the specimen with the naked eyes. This was accompanied by the micro-cracks formation ahead of the crack tip when the load was still below  $P_{ini-Exp}$ . (Fig. 8(b)). Subsequently, the micro-cracks coalesce and the crack growth was observed at about  $P_{ini-Exp}$ . (Fig. 8(c)). As depicted in Fig. 8(d), a load drop was observed when the load reached the maximum and crack propagated after that. Therefore, the mixed mode I/II and mode II delamination onset occurred based on predictions of critical SED approach, and before reaching the critical SERR determined via delamination tests defined in the ASTM standards [8–10].

To detect with a different method at which point during delamination tests initial crack growth onset can take place, the delamination tests were also monitored with acoustic emission system according to the description in Section 3.2 of the present work. To limit the presentation, only for glass/epoxy specimens tested quasi-statically at different mode mixities the changes of load, the energy of each AE hit and cumulative AE energy are illustrated in Fig. 9(a)–(e). To facilitate further analysis, the recorded AE energy per hit for carbon/epoxy specimens has been included in the online dataset accompanying this paper [34]. The green dashed line shows the first nonlinearity point in the load-displacement curve at which the first crack growth was observed. The red<sup>1</sup> dotted line indicates the point at which the first AE hits appeared. Since in this figure, the time has a linear relation with the displacement, the horizontal axis of all graphs can be easily replaced with displacement. The energy of an AE hit was derived as the integral of the squared AE waveform over its duration (energy unit (eu) = 10<sup>-18</sup> J). As it is noticeable in Fig. 9, for all cases, the first AE hits are detected well before the load reaches nonlinearity point as the first observable crack growth point. The value of the load in the first hits is around  $P_{ini-SED}$  summarized in Table 7. According to Fig. 9, as the mode mixity ratio increases, the distance between the green and red lines increases. This can be attributed to the formation of more micro-cracks ahead of the crack tip, which mainly occurs as the mode II loading increases. In addition, there is an accumulation of the AE energy (with a different rate for each mode mixity) between the red and green lines. This amount of accumulated energy contributes to the crack initiation and not to be more than 1% of the total AE energy until the peak load. The accumulation rate increased with loading and different accumulation rates exist due to different mode mixities and the associated failure mechanisms. The AE activities prior to observing the first crack growth on the edge of the test specimen indicates that initial crack growth onset occurs before reaching  $G_{cr|Exp}$ . It should be noted that the choice of AE threshold influences at which point of the load-displacement curve, the first AE signal is detected. Therefore, this parameter can influence the value of  $G$  that is determined as the crack growth onset value based on the AE. Regardless of the exact value of the SERR for crack growth onset obtained by this method, it is definitely clear that this value is lower than  $G_{cr|Exp}$ , obtained via experiments following the ASTM standards [8–10]. This means that crack growth physically starts at  $G < G_{cr|Exp}$ , as predicted by the critical SED approach. Since fiber bridging, as another possible source of AE signals, does not occur before crack growth, the AE activities prior to

<sup>1</sup> For interpretation of color in Fig. 9, the reader is referred to the web version of this article.

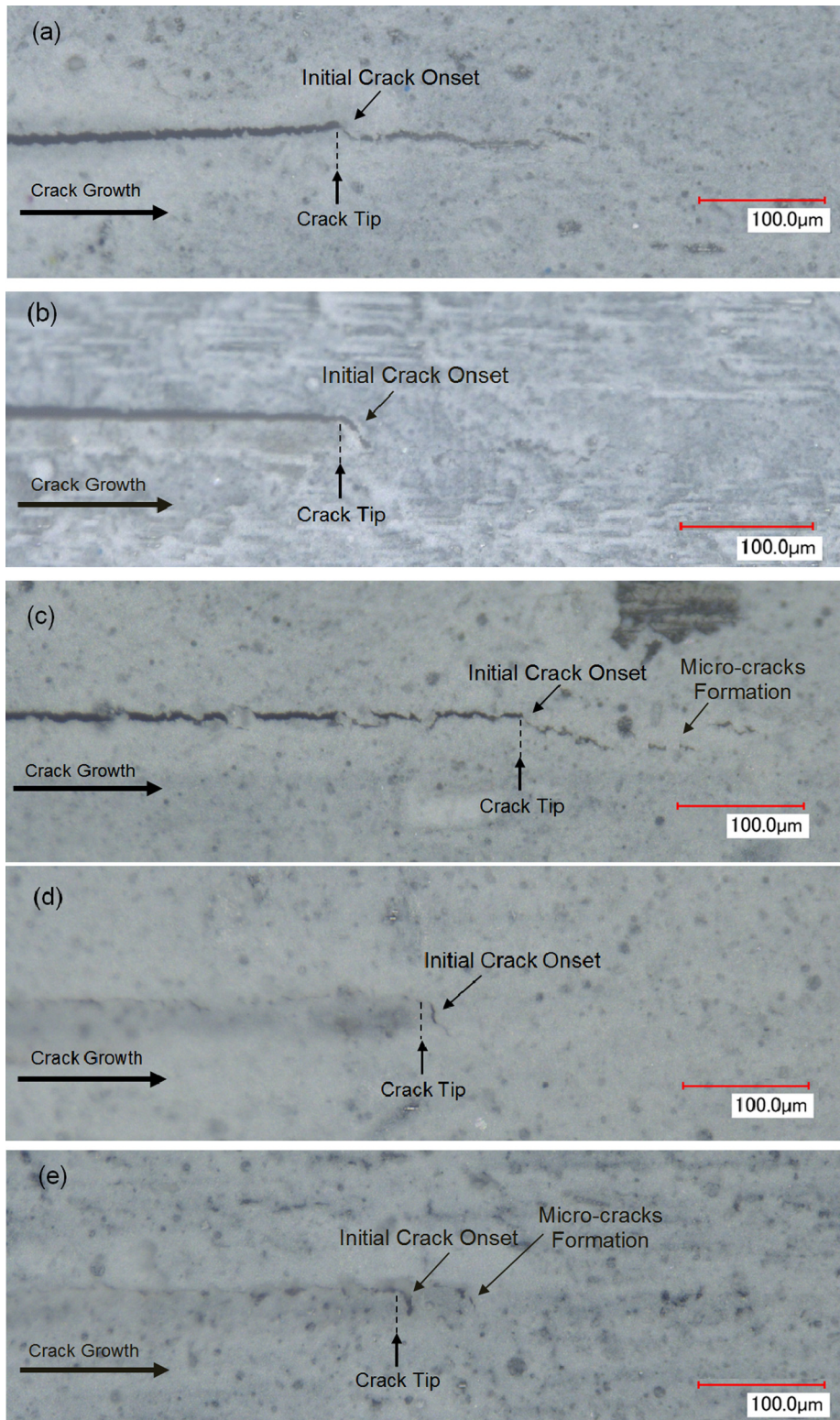


**Fig. 7.** Digital microscopic view of the edge of (a) DCB glass/epoxy, (b) MMB (25%  $G_{II}/G$ ) glass/epoxy, (c) MMB (50%  $G_{II}/G$ ) glass/epoxy, (d) MMB (75%  $G_{II}/G$ ) carbon/epoxy and (e) ENF carbon/epoxy specimens at magnification of  $500\times$ .

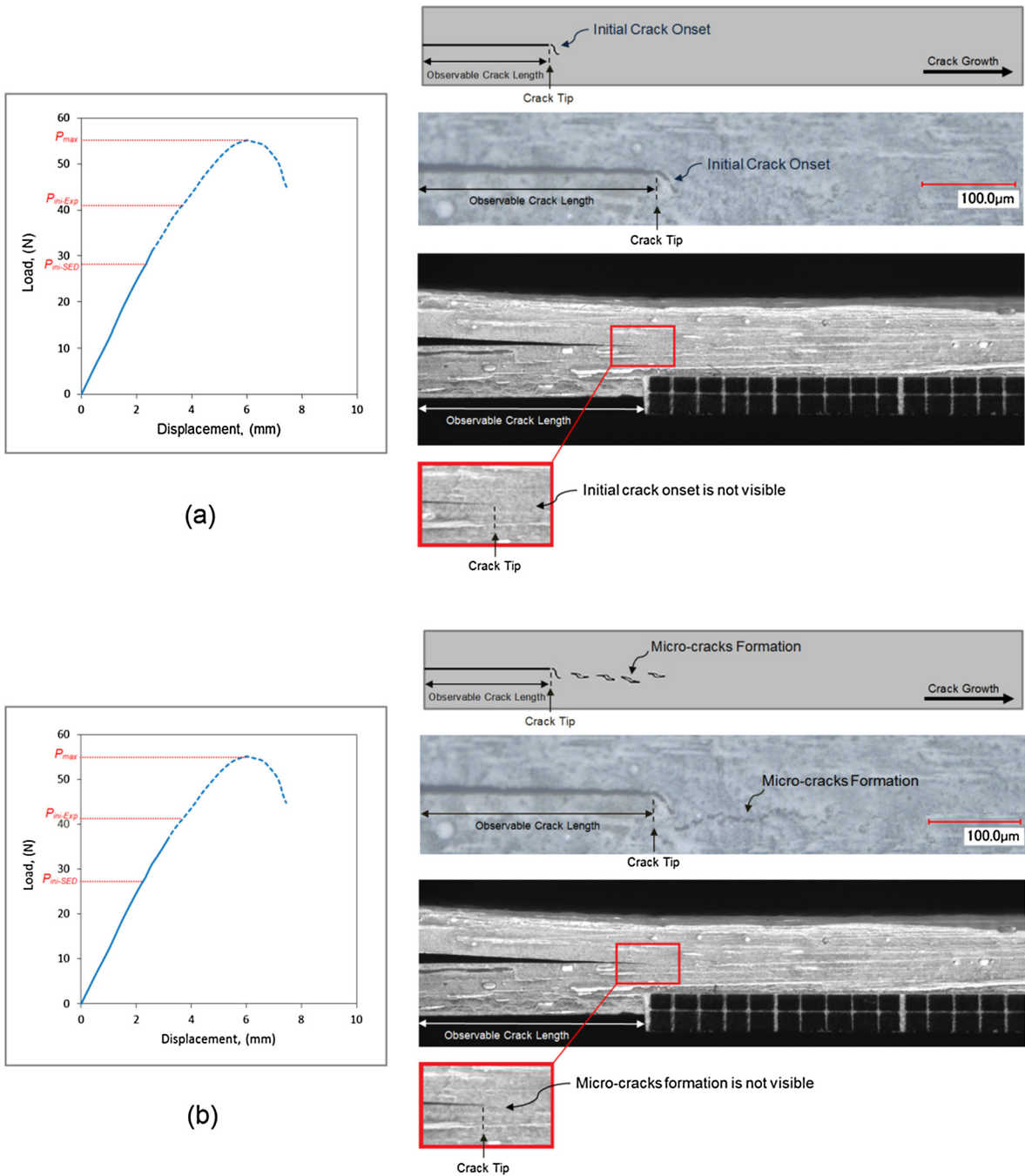
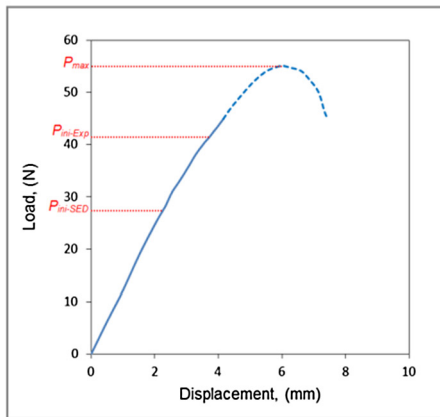


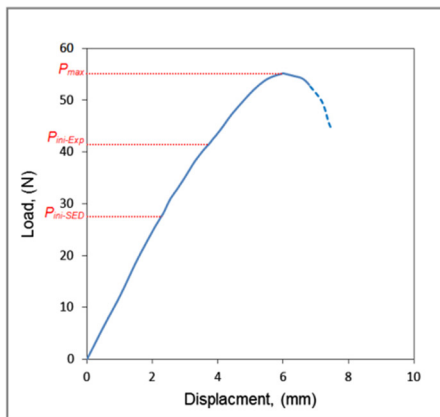
**Fig. 8.** Mixed mode I/II delamination of laminated composite (a) initial crack onset occurs after  $P_{ini-SED}$  is achieved, (b) micro-cracks formation after  $P_{ini-SED}$  and before  $P_{ini-Exp}$ , (c) micro-cracks coalescence and first visible crack growth occurs after  $P_{ini-Exp}$  is achieved and (d) crack propagation.

observable crack growth can be related to micro-cracks formation ahead of the crack tip [35]. This is also suggested by the results of Gutkin et al. [36] who investigated the failure of carbon fiber reinforced plastics using the acoustic emission. By peak frequency analyses, they found that most of the first AE hits correspond to the micro-cracks. Therefore, it would seem logical to consider the difference between  $G_{cr|Exp}$  and  $G_{cr|SED}$  as the energy dissipated by micro-cracks. Further research is needed to investigate this aspect.

From the experimental investigation conducted in the current study, it is concluded that delamination growth initiates earlier than what even nonlinear point can predict. In general, there are four major parts in the load-displacement curve extracted during delamination test. In the first part, the load increases with respect to displacement linearly until the initial crack growth onset (SED point). This linear behavior continues up to the first observable crack growth (nonlinear point). This second part between the SED point and the nonlinear point is attributed to the micro-cracks formation. Following the linear parts, the third part is related to the



(c)



(d)

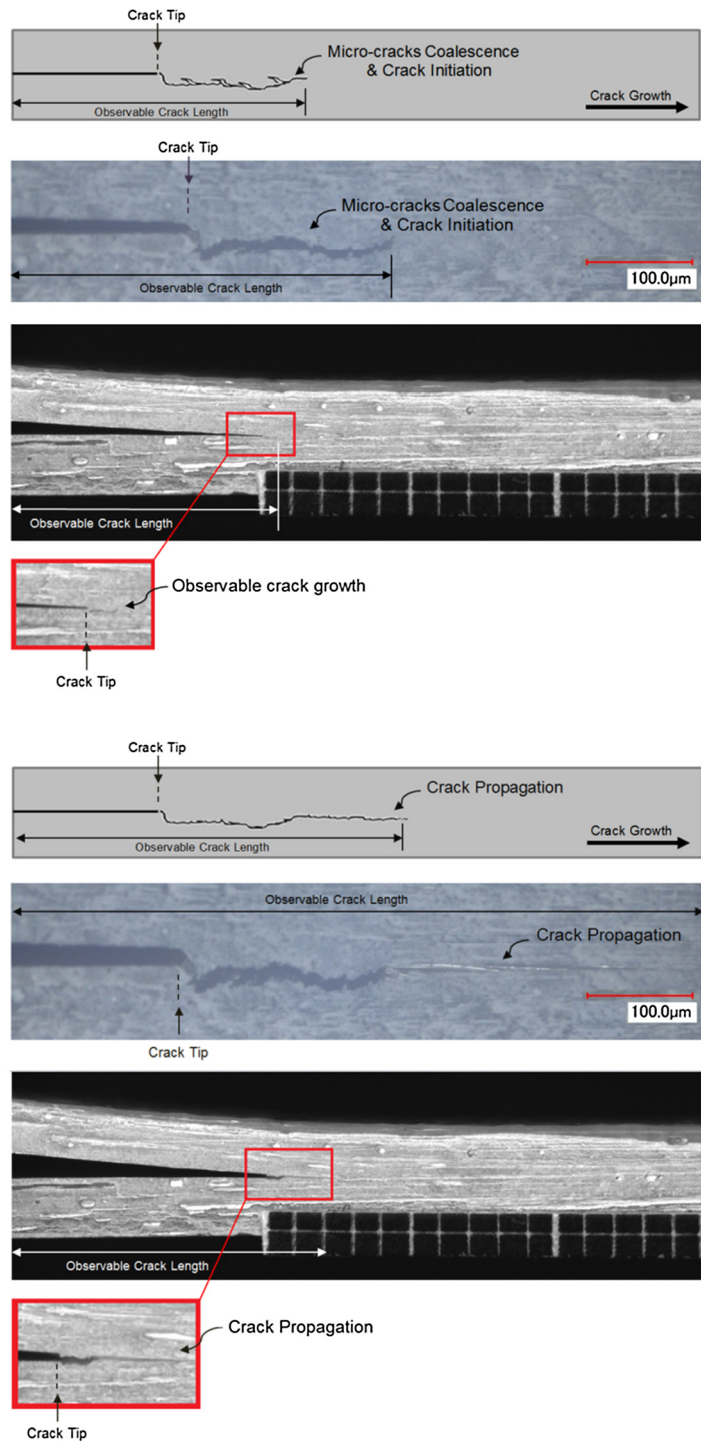
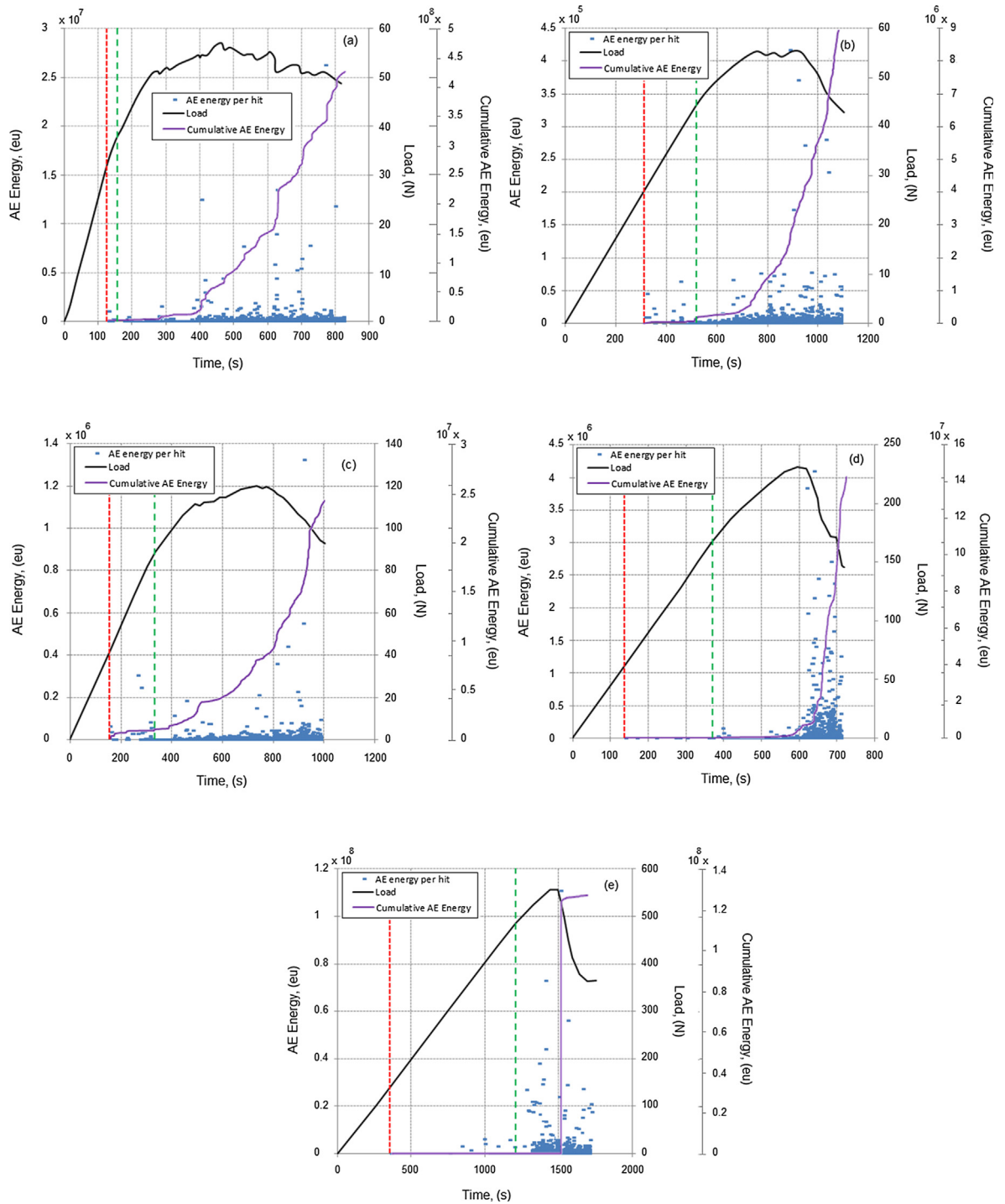


Fig. 8. (continued)

crack propagation and has a nonlinear ascending behavior between the nonlinear point and the maximum load point, which is attributed to the fiber bridging phenomenon. The last part has a nonlinear descending behavior after the maximum load point that indicates the steady-state crack propagation. Further work is necessary to fully understand the link between these parts and micro-mechanisms involved during the delamination growth process.

The question remains, how this knowledge of the microscopic crack growth onset in delamination of laminated composites can be used for engineering purposes? The authors believe that microscopic crack growth onset is important in the design and maintenance of composite structures. When the composite laminates are designed based on  $G_{cr}|_{Exp}$ , as a quasi-static mixed mode I/II delamination



**Fig. 9.** The load, energy of the AE hits, and cumulative AE energy versus time of glass/epoxy specimen under (a) pure mode I, (b) mixed mode I/II (25%  $G_{II}/G$ ), (c) mixed mode I/II (50%  $G_{II}/G$ ), (d) mixed mode I/II (75%  $G_{II}/G$ ) and (e) pure mode II loading.

resistance, some defects, and micro-cracks might be developed ahead of the crack tip although the structure works below  $G_{cr}|_{Exp}$ , but above  $G_{cr}|_{SED}$ . The formation of these defects, especially under fatigue loading has a significant importance, in particular when mode II loading conditions prevail. The growth of fatigue cracks at the SERR levels above  $G_{cr}|_{SED}$  is expected to be faster because the damage has already developed in the fracture process zone. If a quasi-static load prior to fatigue loading with a SERR level above SED onset has been applied, the delamination growth in fatigue may go also when these fatigue loads are below that SERR level. The fatigue crack then coalesces the microcracks present. This may seem important when testing full-scale composite structures where fatigue

load spectra with high peak loads are considered. Therefore, the critical SED approach predicts the level of the load or SERR below which, no damage occurs around the crack tip. This approach is also useful for assurance that no damage is generated ahead of the crack tip during performing compliance calibration tests in specimens by maintaining the SERR level below  $G_{cr|SED}$ .

**5. Conclusion**

The critical SED approach predicts the load at which microscopically the crack onset occurs together with the initial crack growth angle. An experimental investigation of delamination growth in orthotropic composite laminates was conducted, in which the value of the strain energy release rate at the observed crack onset and the angle of the initial crack growth were studied. The quasi-static delamination tests were performed on DCB, MMB and ENF specimens, in order to evaluate the validity of the critical SED approach. Both carbon/epoxy and glass/epoxy specimens were tested for each configuration and examined using a digital microscope to check whether the delamination onset happens. The delamination tests were also monitored with the acoustic emission system to detect at which point during delamination tests initial crack onset can take place. The results showed that the onset of delamination growth occurs before reaching the critical SERR determined via experimental tests following the ASTM standards. The value of critical SERR at delamination initiation obtained via experiments defined in the ASTM standards refers to the coalescence of micro-cracks ahead of the crack tip due to the presence of mode II loading. Only once these micro-cracks coalesce, the macroscopic crack growth can be observed. Moreover, it was shown that the initial crack growth angles predicted for the onset of delamination are in a good agreement with the angles measured using the images taken during experimental tests. This work could provide valuable information about the physics of delamination growth in laminated composites.

**Appendix A**

The intensity of the strain energy density field around the crack tip as the strain energy density factor ( $S$ ) is defined as follows [28]:

$$S = D_1 K_I^2 + D_2 K_{II}^2 + 2D_3 K_I K_{II} \tag{A1}$$

The quantities  $D_i$  ( $i = 1, 2, 3$ ) are given by:

$$\begin{aligned} D_1 &= \frac{1}{4} \left[ \frac{A_I^2}{E_x} + \frac{B_I^2}{E_y} + \frac{C_I^2}{G_{xy}} - \frac{2A_I B_I \nu_{xy}}{E_x} - \frac{A_I^2 \nu_{xz}^2 E_z}{E_x^2} - \frac{B_I^2 \nu_{yz}^2 E_z}{E_y^2} - \frac{2A_I B_I \nu_{xz} \nu_{yz} E_z}{E_x E_y} \right] \\ D_2 &= \frac{1}{4} \left[ \frac{A_{II}^2}{E_x} + \frac{B_{II}^2}{E_y} + \frac{C_{II}^2}{G_{xy}} - \frac{2A_{II} B_{II} \nu_{xy}}{E_x} - \frac{A_{II}^2 \nu_{xz}^2 E_z}{E_x^2} - \frac{B_{II}^2 \nu_{yz}^2 E_z}{E_y^2} - \frac{2A_{II} B_{II} \nu_{xz} \nu_{yz} E_z}{E_x E_y} \right] \\ D_3 &= \frac{1}{4} \left[ \frac{A_I A_{II}}{E_x} + \frac{B_I B_{II}}{E_y} + \frac{C_I C_{II}}{G_{xy}} - \frac{A_I B_{II} \nu_{xy}}{E_x} - \frac{A_{II} B_I \nu_{xy}}{E_x} - \frac{A_I A_{II} \nu_{xz}^2 E_z}{E_x^2} - \frac{B_I B_{II} \nu_{yz}^2 E_z}{E_y^2} - \frac{A_I B_{II} \nu_{xz} \nu_{yz} E_z}{E_x E_y} - \frac{A_{II} B_I \nu_{xz} \nu_{yz} E_z}{E_x E_y} \right] \end{aligned} \tag{A2}$$

The coefficients  $A_i$ ,  $B_i$  and  $C_i$  ( $i = I$  and  $II$ ) are defined as follows [28]:

$$\begin{aligned} A_I &= \text{Re} \left[ \frac{x_1 x_2 (x_2 F_2 - x_1 F_1)}{x_1 - x_2} \right], \quad A_{II} = \text{Re} \left[ \frac{x_2^2 F_2 - x_1^2 F_1}{x_1 - x_2} \right] \\ B_I &= \text{Re} \left[ \frac{x_1 F_2 - x_2 F_1}{x_1 - x_2} \right], \quad B_{II} = \text{Re} \left[ \frac{F_2 - F_1}{x_1 - x_2} \right] \\ C_I &= \text{Re} \left[ \frac{x_1 x_2 (F_1 - F_2)}{x_1 - x_2} \right], \quad C_{II} = \text{Re} \left[ \frac{x_1 F_1 - x_2 F_2}{x_1 - x_2} \right] \end{aligned} \tag{A3}$$

in which

$$F_1 = \frac{1}{(\cos\theta + x_1 \sin\theta)^{\frac{1}{2}}}, \quad F_2 = \frac{1}{(\cos\theta + x_2 \sin\theta)^{\frac{1}{2}}} \tag{A4}$$

where  $\theta$  is the angle from the crack tip, also  $x_1$  and  $x_2$  are roots of the following characteristic equation.

$$C_{11} x^4 - 2C_{16} x^3 + (2C_{12} + C_{66}) x^2 - 2C_{26} x + C_{22} = 0 \tag{A5}$$

The constants  $C_{ij}$  in Eq. (A5) are derived from the following stress-strain relationship ( $\epsilon_i = C_{ij} \sigma_j$ ):

$$\begin{pmatrix} \epsilon_x \\ \epsilon_y \\ \epsilon_z \\ \gamma_{yz} \\ \gamma_{zx} \\ \gamma_{xy} \end{pmatrix} = \begin{pmatrix} 1/E_x & -\nu_{yx}/E_y & -\nu_{zx}/E_z & 0 & 0 & 0 \\ -\nu_{xy}/E_x & 1/E_y & -\nu_{zy}/E_z & 0 & 0 & 0 \\ -\nu_{xz}/E_x & -\nu_{yz}/E_y & 1/E_z & 0 & 0 & 0 \\ 0 & 0 & 0 & 1/G_{yz} & 0 & 0 \\ 0 & 0 & 0 & 0 & 1/G_{zx} & 0 \\ 0 & 0 & 0 & 0 & 0 & 1/G_{xy} \end{pmatrix} \begin{pmatrix} \sigma_x \\ \sigma_y \\ \sigma_z \\ \tau_{yz} \\ \tau_{zx} \\ \tau_{xy} \end{pmatrix} \tag{A6}$$

For plane strain problems, the coefficients  $C_{ij}$  should be replaced by  $C'_{ij}$  as follows:

$$C'_{ij} = C_{ij} - \frac{C_{i3}C_{j3}}{C_{33}} \quad (A7)$$

## References

- [1] Hojo M, Ochiai S, Gustafson CG, Tanaka K. Effect of matrix resin on delamination fatigue crack growth in CFRP laminates. *Eng Fract Mech* 1994;49:35–47.
- [2] Harvey CM, Eplett MR, Wang S. Experimental assessment of mixed-mode partition theories for generally laminated composite beams. *Compos Struct* 2015;124:10–8.
- [3] Tamuzs V, Tarasovs S, Vilks U. Progressive delamination and fiber bridging modeling in double cantilever beam composite specimens. *Eng Fract Mech* 2001;68(5):513–25.
- [4] Blanco N, Gamstedt EK, Asp LE, Costa J. Mixed mode delamination growth in carbon–fibre composite laminates under cyclic loading. *Int J Solids Struct* 2004;41(15):4219–35.
- [5] Shokrieh MM, Daneshjoo Z, Fakoor M. A modified model for simulation of mode I delamination growth in laminated composite materials. *Theor Appl Fract Mech* 2016;82:107–16.
- [6] Sun Y, Yao L, Alderliesten RC, Benedictus R. Mode I quasi-static delamination growth in multidirectional composite laminates with different thicknesses. In: *Proceedings 31st technical conference, American Society for composites*; 2016, p. 1115–25.
- [7] Shokrieh MM, Zeinedini A. A novel method for calculation of strain energy release rate of asymmetric double cantilever laminated composite beams. *Appl Compos Mater* 2014;21(3):399–415.
- [8] ASTM Standard D5528 – 13. Standard test method for mode I interlaminar fracture toughness of unidirectional fiber-reinforced polymer matrix composites. US: ASTM International; 2013.
- [9] ASTM Standard D6671/D6671M – 13e1. Standard test method for mixed mode I-mode II interlaminar fracture toughness of unidirectional fiber reinforced polymer matrix composites. US: ASTM International; 2013.
- [10] ASTM Standard D7905/D7905M – 14. Standard test method for determination of the mode II interlaminar fracture toughness of unidirectional fiber-reinforced polymer matrix composites. US: ASTM International; 2014.
- [11] Mahishi JM. An integrated micromechanical and macromechanical approach to fracture behavior of fiber-reinforced composites. *Eng Fract Mech* 1986;25(2):197–228.
- [12] Hibbs MF, Bradley WL. Correlations between micromechanical failure processes and the delamination toughness of graphite/epoxy systems. In: *Masters J, Au J, editors. Fractography of modern engineering materials: composites and metals, STP948-EB. West Conshohocken, PA: ASTM International; 1987. p. 68–97.*
- [13] Jordan WM, Bradley WL. Micromechanisms of fracture in toughened graphite-epoxy laminates. In: *Johnston N, editor. Toughened composites, STP937-EB. West Conshohocken, PA: ASTM International; 1987. p. 95–114.*
- [14] Hashemi S, Kinloch AJ, Williams JG. Mechanics and mechanisms of delamination in a poly(ether sulphone)-fibre composite. *Comp Sci Technol* 1990;37(4):429–62.
- [15] Greenhalgh ES, Rogers C, Robinson P. Fractographic observations on delamination growth and the subsequent migration through the laminate. *Compos Sci Technol* 2009;69:2345–51.
- [16] Bonhomme J, Arguelles A, Viña J, Viña I. Fractography and failure mechanisms in static mode I and mode II delamination testing of unidirectional carbon reinforced composites. *Polym Test* 2009;28:612–7.
- [17] Daneshjoo Z, Shokrieh MM, Fakoor M. A micromechanical model for prediction of mixed mode I/II delamination of laminated composites considering fiber bridging effects. *Theor Appl Fract Mech* 2018;94:46–56.
- [18] Datta S. Investigation of the micromechanics of delamination in fibre reinforced composites PhD. Thesis UK: Imperial College; 2005.
- [19] Amaral L, Alderliesten RC, Benedictus R. Towards a physics-based relationship for crack growth under different loading modes. *Eng Fract Mech* 2018;195:222–41.
- [20] Daneshjoo Z. Delamination of laminated composites under mixed mode I/II loading considering the fracture process zone effects PhD. Thesis Iran University of Science and Technology; 2018.
- [21] Erdogan F, Sih GC. On the crack extension in plates under plane loading and transverse shear. *J Basic Eng* 1963;85(4):519–25.
- [22] Hussain MA, Pu SL, Underwood J. Strain energy release rate for a crack under combined mode I and mode II. In: *Irwin G, editor. Fracture analysis: proceedings of the 1973 national symposium on fracture mechanics, Part II, STP560-EB. West Conshohocken, PA: ASTM International; 1974. p. 2–28.*
- [23] Sih GC. Strain-energy-density factor applied to mixed mode crack problems. *Int J Fract* 1974;10(3):305–21.
- [24] Jernkvist LO. Fracture of wood under mixed mode loading: I. Derivation of fracture criteria. *Eng Fract Mech* 2001;68(5):549–63.
- [25] Fakoor M, Rafiee R. Fracture investigation of wood under mixed mode I/II loading based on the maximum shear stress criterion. *Strength Mater* 2013;45(3):378–85.
- [26] Fakoor M, Khansari NM. Mixed mode I/II fracture criterion for orthotropic materials based on damage zone properties. *Eng Fract Mech* 2016;153:407–20.
- [27] Sih GC, Michopoulos JG, Chou SC. The strain energy density function. In: *Sih GC, Michopoulos JG, Chou SC, editors. Hygrothermoelasticity. Dordrecht: Springer; 1986.*
- [28] Sih GC, Paris PC, Irwin GR. On cracks in rectilinearly anisotropic bodies. *Int J Fract Mech* 1965;1(3):189–203.
- [29] Sih GC. Mechanics of fracture initiation and propagation: surface and volume energy density applied as failure criterion. Springer Science & Business Media; 2012.
- [30] Khan R. Delamination growth in composites under fatigue loading PhD. Thesis Aerospace Faculty TU Delft Nederland; 2013.
- [31] Shokrieh MM, Salamat-talab M, Heidari-Rarani M. Effect of interface fiber angle on the R-curve behavior of E-glass/epoxy DCB specimens. *Theo Appl Fract Mech* 2016;86:153–60.
- [32] ImageJ. An open platform for scientific image analysis. < <https://imagej.net> >; 2009 [accessed 28 August 2018].
- [33] Amaral L, Zarouchas DS, Alderliesten RC, Benedictus R. Energy dissipation in mode II fatigue crack growth. *Eng Fract Mech* 2017;173:41–54.
- [34] Daneshjoo Z, Alderliesten RC, Shokrieh MM, Fakoor M. The physics of delamination onset in orthotropic composite laminates under mixed mode I/II loading; 2018. <https://doi.org/10.4121/uuid:4e9c1af6-dcfa-4992-a18a-4b24fd5180f8>.
- [35] Nikbakht M, Yousefi J, Hosseini-Toudeshky H, Minak G. Delamination evaluation of composite laminates with different interface fiber orientations using acoustic emission features and micro visualization. *Compos Part B: Eng* 2017;113:185–96.
- [36] Gutkin R, Green CJ, Vangrattanachai S, Pinho ST, Robinson P, Curtis PT. On acoustic emission for failure investigation in CFRP: pattern recognition and peak frequency analyses. *Mech Syst Signal Process* 2011;25:1393–407.